17

Electromagnetic Wave Absorption Properties of RE-Fe Nanocomposites

Ying Liu, LiXian Lian and Jinwen Ye
Sichuan University
China

1. Introduction

Recently, the number of communication devices that utilize gigahertz range microwave radiation, such as mobile phones and LAN systems, has greatly increased. However, electromagnetic interference (EMI) has become serious. One promising technique to prevent EMI is the use of microwave absorption materials. However, the applications of conventional microwave absorption materials are limited. The reasons are that Snoek's limit of spinel-tripe ferrites is so small that the imaginary part of permeability is considerably lowered in GHz range, and metallic soft-magnet materials have high electric conductivity, which makes the high frequency permeability decreased drastically due to the eddy current loss induced by EM wave.

The $Nd_2Fe_{14}B$/α-Fe composites is composed of soft magnetic α-Fe phase with high M_S and hard magnetic $Nd_2Fe_{14}B$ phase with large H_A, consequently their natural resonance frequency are at a high frequency range and permeability still remains as a large value in high frequency range. Furthermore, the electric resistivity of $Nd_2Fe_{14}B$ is higher than that of metallic soft magnetic material, which can restrain the eddy current loss. Thus, the authors have already reported that $Nd_2Fe_{14}B$/α-Fe composites can fuction as a microwave absorber. In this present work, the electromagnetic and absorption properties of the $Nd_2Fe_{14}B$/α-Fe nanocomposites were studied in the 0.5–18 and 26.5–40 GHz frequency ranges. Moreover, the effect of rare earth Nd content on natural resonance frequency and microwave permeability of $Nd_2Fe_{14}B$/α-Fe nanocomposites was reported in this chapter. The results show that it is possible to be a good candidate for thinner microwave absorbers in the GHz range.

In order to restrain the eddy current loss of metallic soft magnetic material, Sm_2O_3 and SmN was introduced in Sm_2O_3/α-Fe and SmN/α-Fe composites as dielectric phase, and $Sm_2Fe_{17}N_x$ with high magnetocrystalline anisotropy was introduced in SmN/α-Fe/$Sm_2Fe_{17}N_x$ as hard magnetic phase. Accordingly, Sm_2O_3/α-Fe and SmN/α-Fe/$Sm_2Fe_{17}N_x$ are possible to be another good candidate for microwave absorbers in the GHz range as the authors reported in reference. Therefore, the purpose of this study is to investigate the microwave complex permeability, resonant frequency, and microwave absorption properties of nanocrystalline rare-earth magnetic composite materials Sm_2O_3/α-Fe and SmN/α-Fe/$Sm_2Fe_{17}N_x$. The absorption performance and natural resonance frequency can be controlled by adjusting phase composite proportion and optimizing the microstructure.

II. Microwave Electromagnetic Properties of $Nd_2Fe_{14}B$/α-Fe

1. Experiments

The compounds NdFeB alloys were induction-melted under an argon atmosphere. The ribbons were prepared by the single-roll melt-spun at a roll surface velocity of 26 m/s, and then annealed at 923-1023K for 8-20 min in an argon atmosphere. The annealed ribbons were pulverized for 10-30h using a planetary ball milling machine. X-ray diffraction (XRD) and transmission electron microscope (TEM) were used to determine the phases and microstructure of samples. The magnetic hysteresis loops were measured using a vibrating sample magnetometer (VSM). The alloy powders were mixed with paraffin at a weight ratio of 5:1 and compacted respectively into a toroidal shape (7.00 mm outer diameter, 3.01 mm inner diameter and approximately 3 mm thickness.) and rectangular shape (L×W= 7.2×3.6: corresponding to the size of various wave guide, thickness: 0.9 mm). The vector value of reflection/transmission coefficient (scattering parameters) of samples were measured in the range of 0.5-18 GHz and 26.5-40 GHz, using an Agilent 8720ET and Agilent E8363A vector network analyzer respectively. The relative permeability (μ_r) and permittivity (ε_r) values were determined from the scattering parameters and sample thickness. Assumed the metal material was underlay of absorber, and the reflection loss (RL) curves were calculated from the relative complex permeability and permittivity with a given frequency range and a given absorber thickness (d) with the following equations:

$$RL = 20\log\left|(Z_{in}-1)/(Z_{in}+1)\right| \tag{1}$$

$$Z_{in} = \sqrt{\mu_r/\varepsilon_r}\tanh\left\{j(2\pi fd/c)\sqrt{\mu_r\varepsilon_r}\right\} \tag{2}$$

, where Z_{in} is the normalized input impedance at absorber surface, f the frequency of microwave, and c the velocity of light.

2. Microwave electromagnetic properties of $Nd_{10}Fe_{78}Co_5Zr_1B_6$

In the present work, $Nd_2Fe_{14}B$/α-Fe microwave electromagnetic and absorption properties of $Nd_2Fe_{14}B$/α-Fe were investigated in 0.5-18 and 26.5-40GHz range.

Fig.1 (a) and Fig.1 (b) show the XRD patterns of the $Nd_{10}Fe_{84}B_6$ melt-spun ribbons after subsequent annealing and ball milling respectively. The peaks ascribed to hard magnetic phase $Nd_2Fe_{14}B$ and soft magnetic phase α-Fe can be observed clearly. After ball milling, the diffraction peaks exhibit the wider line broadening, and any other phase has not been detected on the XRD patterns. It indicates the grain size gets finer by ball-milling. The average grain size is evaluated to be about 30nm for annealed ribbons and 20nm for the ball-milling one from the line broadening of the XRD peaks, using the Scherrer's formula. Fig.2. shows TEM micrograph and electron diffraction (ED) patterns of the heat treated $Nd_{10}Fe_{78}Co_5Zr_1B_6$ melt-spun ribbons. It can be seen that the grain size is uniform and the average diameter is around 30 nm. The results are consistent with the XRD analysis. Such a microstructure of magnetic phase is effective to enhance the exchange interaction between hard and soft magnetic phases.

Magnetic hysteresis loop for $Nd_2Fe_{14}B$/α-Fe nanocomposites is shown in Fig.3. The value of saturation magnetization M_s and coercivity H_{cb} is 100.03 emu/g and 2435 Oe

respectively, which is rather high compared with common soft magnetic materials such as hexaferrite - FeCo nanocomposite. Furthermore, the magnetic hysteresis loops are quite smooth, which shows the characteristics of single phase hard magnetic material. This result can be explained by the effect of exchange interaction between the hard-magnetic $Nd_2Fe_{14}B$ and soft-magneticα-Fe. Comparing with conventional ferrite materials, the $Nd_2Fe_{14}B$/α-Fe permanent magnetic materials has larger saturation magnetization value and its snoek's limit is at 30-40GHz. Thus the values of relative complex permeability can still remain rather high in a higher frequency range.

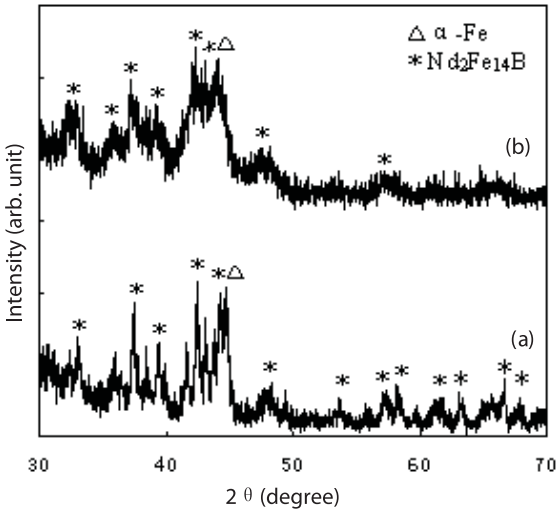

Fig. 1. XRD patterns of $Nd_{10}Fe_{78}Co_5Zr_1B_6$ composite melt-spun ribbons annealed at 973K for 8 min before (a) and after 25h milling (b)

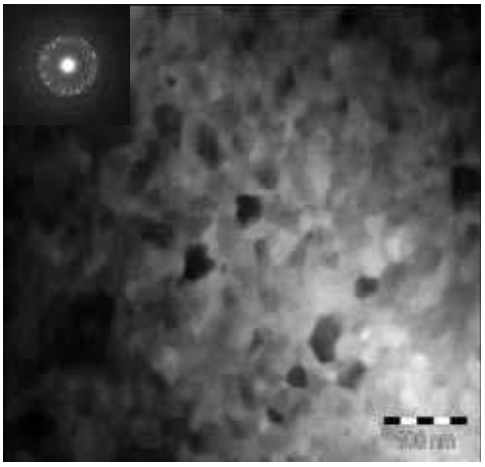

Fig. 2. TEM micrograph and diffraction patterns of the heat treated $Nd_{10}Fe_{78}Co_5Zr_1B_6$ melt-spun ribbons

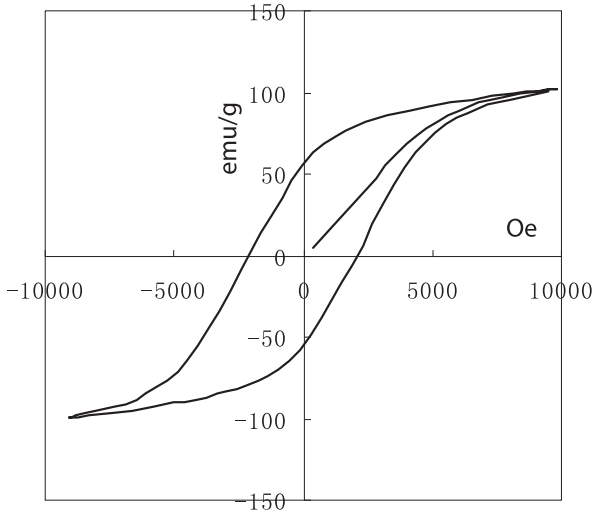

Fig. 3. Magnetic hysteresis loop for $Nd_2Fe_{14}B$/α-Fe nanocomposite

Fig.4 shows the frequency dependence of the complex relative permeability and permittivity of $Nd_2Fe_{14}B$/α-Fe composites. As shown in Fig.4 (a) and (b), that values of complex permittivity decrease with increasing frequency for $Nd_2Fe_{14}B$/α-Fe composites in 0.5-18 GHz. However the imaginary part of permittivity ε_r'' exhibits a peak at 36 GHz. The dielectric constant of $Nd_2Fe_{14}B$/α-Fe composites are higher than that of ferrites due to high electric conductivity of metal material α-Fe, and the dielectric loss plays an important role in microwave absorption property. The dielectric properties of $Nd_2Fe_{14}B$/α-Fe composites arise mainly from the interfacial polarization induced by the large number of interface for nanocomposites. However low complex dielectric constant of $Nd_2Fe_{14}B$/α-Fe composites is expected to satisfy the requirements of impedance matching. The permeability spectra of $Nd_2Fe_{14}B$/α-Fe nanocomposites exhibits relaxation and resonance type characteristic in the 0.5-18 and 26.5-40 GHz frequency range respectively. The resonance frequency (f_r) of $Nd_{10}Fe_{78}Co_5Zr_1B_6$ nanocomposite is 30GHz due to the large anisotropy field (H_A). It is well known that the ferromagnetic resonance frequency (f_r) is related to its anisotropy fields (H_A) by the following relation:

$$2\pi f_r = \gamma H_A \tag{3}$$

,where γ is the gyromagnetic ratio. $Nd_2Fe_{14}B$/α-Fe nanocomposites have a large anisotropy field H_A, and consequently their natural resonance frequency f_r is at a high frequency range. The resonance frequency of $Nd_2Fe_{14}B$ is calculated as 210GHz. However, the resonance frequency of this $Nd_2Fe_{14}B$/α-Fe sample is lower than that of $Nd_2Fe_{14}B$, due to the decrease of H_A induced by the exchange interaction between hard and soft magnetic phases. Thus the observed resonance phenomena in Fig.4(c) can be attributed to the resistance to the spin rotational. And the ferromagnetic resonance plays an important role in the high frequency region.

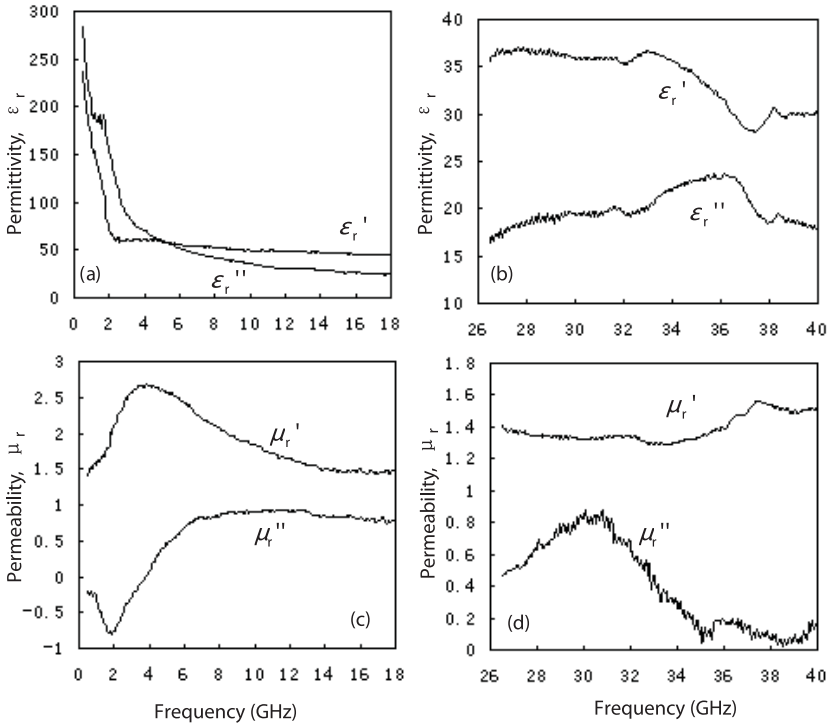

Fig. 4. The relative permittivity and permeability plotted against frequency for $Nd_2Fe_{14}B/\alpha$-Fe composites in the 0.5-18 and 26.5-40GHz

The variation of reflection loss with frequency for composite is shown in Fig.5. This nanocomposite realized the optimum matching (reflection loss: RL < -20 dB) in 9, 17 GHz with thin matching thickness of 2, 1.2 mm respectively. Furthermore, the maximum microwave absorption -35 dB is obtained at 37 GHz with a thinner matching thickness (d_m) of 0.37 mm. Consequently, efficient EM absorption properties are observed not only in centimeter-wave band but also in millimeter-wave band.

The permeability spectra of $Nd_2Fe_{14}B/\alpha$-Fe nanocomposites exhibits relaxation and resonance type characteristic in the 0.5-18 and 26.5-40 GHz frequency range respectively. The resonance frequency (f_r) of $Nd_{10}Fe_{78}Co_5Zr_1B_6$ nanocomposite is 30GHz. This nanocomposite also shows an excellent microwave absorption property (reflection loss: RL<-20dB) in 9, 17 GHz with thin matching thickness of 2, 1.2mm respectively, and the minimum peak of -35 dB appears at 37 GHz with a thin matching thickness (dm) of 0.37 mm.

3. Effect of Nd content on natural resonance frenquency and microwave permeability of $Nd_2Fe_{14}B/\alpha$-Fe nanocomposites

The natural resonance frequency (f_r) is related to its anisotropy fields (H_A) by the expression (3).

$$2\pi f_r = \gamma H_A \tag{3}$$

where γ is the gyromagnetic ratio. And there is a relationship between the absorber thickness d_m and magnetic loss μ_r'' of absorbers by

$$d_m = c / 2\pi f_m \mu_r'' \tag{4}$$

where c is velocity of light and f_m is the matching frequency. Therefore, the magnetic materials which show higher μ_r'' values are suitable for the fillers of thinner microwave absorbers. However, the maximum μ_r'' value induced by natural resonance phenomenon is estimated using the saturation magnetization M_s and H_A as

$$\mu_r'' = M_s / 3\mu_0 H_A \alpha \tag{5}$$

where μ_0 is the permeability of vacuum state and α is Gilbert's damping coefficient. Consequently, d_m is inversely proportion to M_s from formulae (2) and (3), and it is effective to use a metal-based material with high M_s and adequate f_r values, such as $Nd_2Fe_{14}B$/α-Fe nanocomposites due to the high M_s of α-Fe (M_s = 2.15T) and the large H_A of $Nd_2Fe_{14}B$ (H_A =6.0MAm^{-1}). T. Maeda et al investigated the effect of exchange interaction between the hard-magnetic $Y_2Fe_{14}B$ and soft-magnetic Fe_3B on the resonance phenomenon. Kato et al. also reported a shift of the ferromagnetic resonance (FMR) frequency by changing the volume fraction of soft and hard phases in the $Nd_2Fe_{14}B$/α -Fe thin films. Therefore, it is possible to control the f_r values of $Nd_2Fe_{14}B$/α -Fe nanocomposites by changing the rare earth Nd content. Due to the effect of exchange interaction, nanocrystalline composites $Nd_2Fe_{14}B$/α-Fe magnet with high theoretical energy product $(BH)_{max}$ value attract much attention as permanent magnet.

In the present work, the effect of the rare earth Nd contents on the natural resonance frequency and microwave permeability of $Nd_2Fe_{14}B$/α-Fe nanocomposites was investigated. The $Nd_xFe_{94-x}B_6$ (x = 9.5, 10.5, 11.5) ribbons were prepared using melt-spinning and annealing method. The microwave complex permeability was measured in the 26.5-40 GHz frequency range.

Fig.6 shows the XRD patterns of the heat treated $Nd_xFe_{94-x}B_6$ melt-spun ribbons with different Nd contents. The peaks ascribed to hard magnetic phase $Nd_2Fe_{14}B$ and soft magnetic phaseα-Fe have been observed clearly. The average grain size D calculated by using Scherrer equation are about 30nm for $Nd_xFe_{94-x}B_6$ (x=9.5, 10.5, 11.5) composites. Furthermore, it is noticeable that the fraction of $Nd_2Fe_{14}B$ are gradually increased and the fraction of α-Fe are gradually decreased with the increasing of the Nd content based on checking the ratio of characteristic peaks intensity of $Nd_2Fe_{14}B$ to that of α-Fe. Thereby, the magnetic properties of $Nd_2Fe_{14}B$/α-Fe nanocomposite powder with different Nd content exhibit obvious differences as shown in Fig.7.

The values of remanent magnetization and coercivity are very high compared with soft magnetic materials, and the magnetic hysteresis loops are quite smooth. It behaves the characteristics of single hard magnetic material. This result can be explained by the effect of exchange interaction between the hard-magnetic $Nd_2Fe_{14}B$ and soft-magneticα-Fe. Fig.8. shows TEM micrograph and electron diffraction (ED) patterns of the heat treated $Nd_{9.5}Fe_{84.5}B_6$ melt-spun ribbons. It can be seen that the grain size is uniform and the average diameter is around 30 nm. The results are consistent with the XRD analysis. Such a

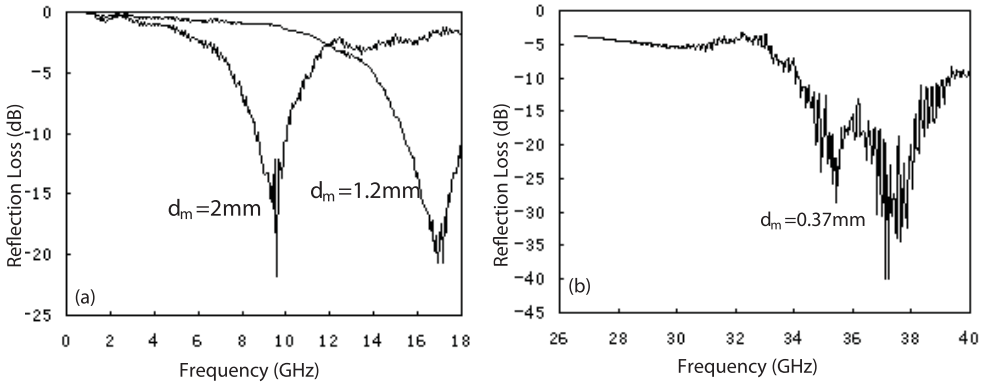

Fig. 5. Frequency dependences of RL of $Nd_2Fe_{14}B$/α-Fe composite in (a) 0.5-18GHz and (b) 26.5-40GHz

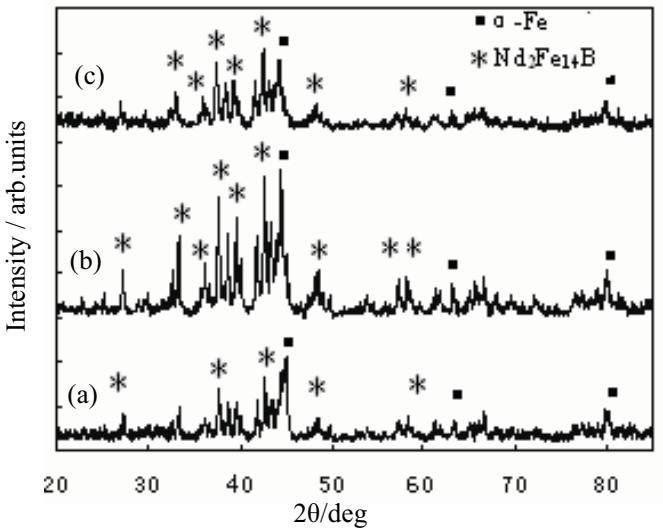

Fig. 6. XRD patterns of $Nd_xFe_{94-x}B_6$ (a) x=9.5, (b) x=10.5, and (c) x=11.5 melt-spun ribbons annealed at 973K for 8 min

microstructure of small grains of magnetic phase is available to enhance the exchange interaction between hard and soft magnetic phases. Because the exchange interaction is only efficient in surface shell, approximately within a diameter of the Block wall width δ_B, this extremely fine-grained microstructures is necessary to ensure that a considerable volume fraction of grain is affected by the exchange coupling.

At the same time, the saturation magnetization M_s is gradually decreased and the coercivity H_c is gradually increased with the increase of the Nd content, due to the decrease of volume fraction of soft-magneticα-Fe phases with high M_s and the increasing of the volume fraction of hard-magnetic $Nd_2Fe_{14}B$ phases with high H_A (see Fig.6).

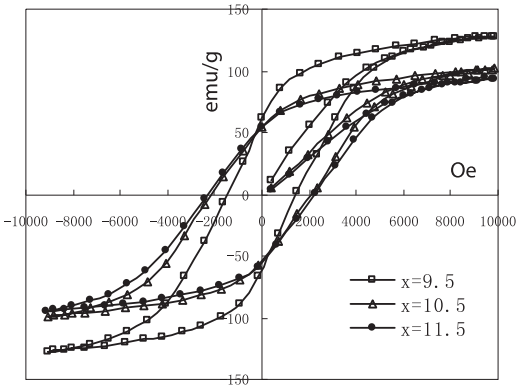

Fig. 7. Magnetic hysteresis loops for $Nd_2Fe_{14}B/\alpha$-Fe nanocomposites powder with different Nd content

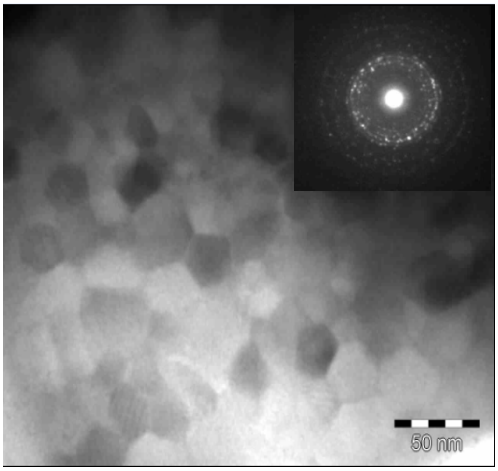

Fig. 8. TEM micrograph and diffraction patters of the heat treated $Nd_xFe_{94-x}B_6$(x=9.5) melt-spun ribbons

Because M_s and effective anisotropy constant K_{eff} are depended on the volume fraction of soft-magnetic phases f_S and that of hard-magnetic phases as shown in Eq. (6) and (7),

$$Ms = f_S M_S^S + (1 - f_S) M_S^H \tag{6}$$

$$\begin{aligned} K_{\text{eff}} &= \int \varphi(\gamma) K_1(\gamma) \varphi(\gamma) d\gamma \\ &=< K_1(\gamma) >= f_S K_S + (1 - f_S) K_H \end{aligned} \tag{7}$$

where M_S^S and K_S are the saturation magnetization and anisotropy constant of soft-magneticα -Fe phases respectively, M_S^H and K_H are the saturation magnetization and anisotropy constant of hard-magnetic $Nd_2Fe_{14}B$ phases respectively. Therefore microwave

permeability and the resonance frequency f_r will exhibit obvious differences with different Nd content.

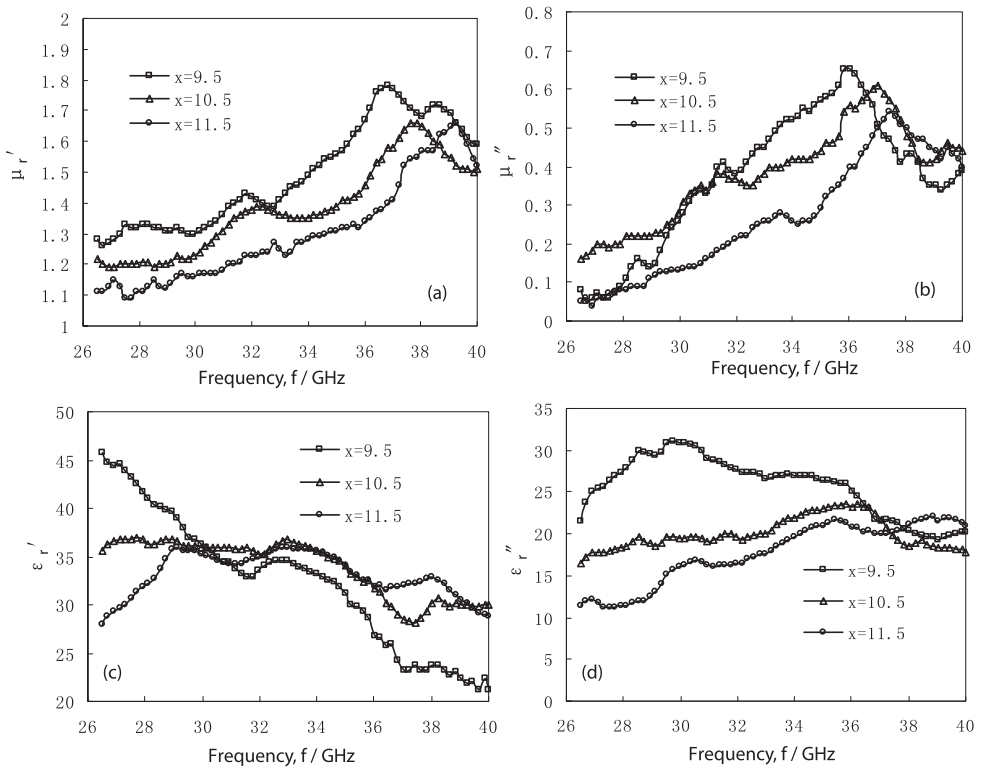

Fig. 9. The frequency dependencies of the complex relative permeability and permittivity of resin composites $Nd_xFe_{94-x}B_6$(x=9.5, 10.5, 11.5):
(a) real part μr′ of complex permeability; (b) imaginary part μ_r" of complex permeability;

Fig.9 shows the frequency dependencies of the complex relative permeability and permittivity of resin composites $Nd_xFe_{94-x}B_6$(x=9.5, 10.5, 11.5). Compared with hexagonal W-type ferrites reported in reference, $Nd_2Fe_{14}B$/α-Fe nanocomposites shows higher values in both the real μ_r'and imaginary μ_r" parts of permeability in the higher frequency region. These higher values are due to the larger magnetization of $Nd_2Fe_{14}B$/α-Fe than ferrites. For Nd9.5Fe84.5B6 resin composites, the maximum of μ_r" is 0.65 and the resonance frequency is around 36GHz. For $Nd_{10.5}Fe_{83.5}B_6$ and $Nd_{11.5}Fe_{82.5}B_6$ samples, the maxima of μ_r" are 0.61 and 0.54, and f_r are 37GHz and 37.5GHz respectively. It shows that the μ_r" values of $Nd_xFe_{94-x}B_6$ for x=10.5 and x=11.5 are smaller than that of $Nd_{9.5}Fe_{84.5}B_6$ sample, whereas the resonance frequency f_r of these two composites are higher than that of the $Nd_{9.5}Fe_{84.5}B_6$ sample. This interesting resonance phenomenon could be explained as follows. On the one hand, the volume fractions of soft-magneticα-Fe phase with higher M_s decreases with the increase of rare earth Nd content (shown in Fig.6), resulting in the decrease of μ_r" based on

Eq. (5). On the other hand, the volume fractions of hard-magnetic $Nd_2Fe_{14}B$ phase with higher HA increases gradually. As a result, resonance frequency f_r shifts to a higher frequency range with the increase of rare earth Nd content, according to Eq. (3)..

$Nd_2Fe_{14}B$/α-Fe composites have much larger H_A than common absorber materials such as ferrites and metal soft magnetic materials, and behave the characteristics of hard magnetic material. Therefore magnetic spectrum of $Nd_2Fe_{14}B$/α-Fe composites shows some difference with other absorber materials, and the real μ_r' doesn't decrease with frequency in the resonance region as general rule. The detailed reasons are expected to be investigated.

It can be seen from Fig.9 (c) and Fig.9 (d), that values of the real part of complex permittivity ε_r' are found to decrease with increasing frequency for $Nd_xFe_{94-x}B_6$ composites. The imaginary part of permittivity ε_r'' exhibits a peak at 30GHz ,35GHz and 38GHz for $Nd_xFe_{94-x}B_6$(x=9.5, 10.5, 11.5) respectively. It can be seen that the dielectric constant are higher than ferrites, the dielectric loss play an important role in microwave absorption property. Thus, microwave absorption properties of $Nd_2Fe_{14}B$/α-Fe composites depend on cooperate effect of magnetic loss and dielectric loss. The dielectric properties of $Nd_2Fe_{14}B$/α-Fe composites arise mainly due to the interfacial polarization. It also shows that the complex dielectric constant is composition dependent. However low complex dielectric constant of $Nd_2Fe_{14}B$/α-Fe composites is expected to satisfy the requirements of impedance matching.

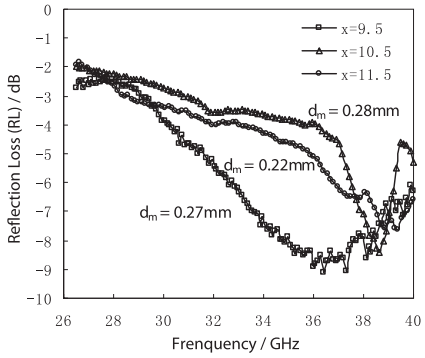

Fig. 10. Frequency dependence of RL for the resin composites NdxFe94-xB6 (x=9.5, 10.5, 11.5)

Finally, the RL of the resin composites $Nd_xFe_{94-x}B_6$ (x=9.5, 10.5, 11.5) are calculated from the microwave complex permeability and permittivity, and absorber thickness. Their frequency dependence is shown in Fig.10.The optimum matching condition is realized when absorber thickness is 0.27mm and a minimum RL value of -8.9dB is obtained at the f_m of 36GHz for the $Nd_{9.5}Fe_{84.5}B_6$ sample. For $Nd_{10.5}Fe_{83.5}B_6$ and $Nd_{11.5}Fe_{82.5}B_6$ composites, the f_m are 38.6GHz and 39.4GHz respectively, and higher than that of the $Nd_{9.5}Fe_{84.5}B_6$ sample. This is attribute to the increase in H_A due to the increase of hard-magnetic $Nd_2Fe_{14}B$ phases. This result is in good agreenment with the results from Fig.9. Further more, $Nd_2Fe_{14}B$/α-Fe composites have a thinner matching thickness than ferrites absorber materials demonstrated by Y. J.

The microwave permeability and the frequency range of microwave absorption of $Nd_2Fe_{14}B$/α-Fe nanocomposites can be controlled effectively by adjusting rare earth Nd content. Microwave permeability reduces and natural resonance frequency f_r shifts to a

higher frequency with the increase of Nd content. $Nd_{9.5}Fe_{84.5}B_6$ resin composites shows the maximum μ_r'' of 0.65 at 36GHz and the maximum microwave absorption(RL=-8.9dB) is obtained at 36GHz with the matching thickness of 0.27mm. $Nd_2Fe_{14}B$/α-Fe nanocomposites are promising microwave absorbers in the 26.5-40GHz frequency range.

4. Electromagnetic wave absorption properties of NdFeB alloys with low Nd content

In this section, the electromagnetic and absorption properties of NdFeB alloys with low Nd content comprised withα-Fe /$Nd_2Fe_{14}B$ nanocomposites were studied in the 0.5–18 GHz frequency ranges.Fig.11 shows the XRD patterns of $Nd_6Fe_{91}B_3$ melt-spun ribbons after annealing at 1073K for 15 min. The peaks ascribed to soft magnetic phaseα-Fe and hard magnetic phase $Nd_2Fe_{14}B$ have been observed clearly. The average grain size D calculated by using Scherrer equation are about 35nm forα-Fe phase.

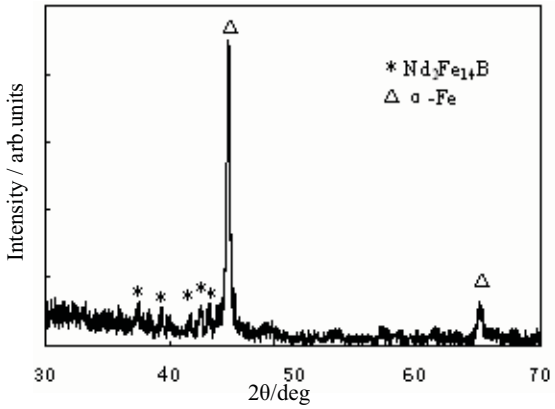

Fig. 11. XRD patterns of $Nd_6Fe_{91}B_3$ melt-spun ribbons annealed at1073K for 15 min

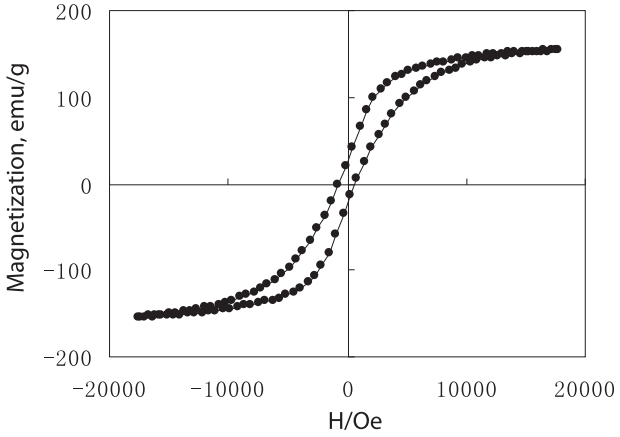

Fig. 12. Magnetic hysteresis loops for $Nd_6Fe_{91}B_3$ compositions after annealing at 1073K

Magnetic hysteresis loop for $Nd_2Fe_{14}B/\alpha$-Fe nanocomposites is shown in Fig.12. The value of saturation magnetization M_s and coercivity H_{cb} is 154.35 emu/g and 667 Oe respectively. The values of remanent magnetization and coercivity are very high compared with common soft magnetic materials such as hexaferrite - FeCo nanocomposite. Furthermore, the magnetic hysteresis loops are quite smooth and it behaves the characteristics of single hard magnetic material. This result can be explained by the effect of exchange interaction between the hard-magnetic $Nd_2Fe_{14}B$ and soft-magnetic α-Fe.

Fig.13 shows the frequency dependence of relative permeability, permittivity. For $Nd_6Fe_{91}B_3$ composites, the real part μ' and imaginary part μ_r'' of relative permeability shows two dispersion peaks, and the first peak may induced by the size resonance due to the inhomogeneous of composites. The permeability spectra of $Nd_2Fe_{14}B/\alpha$-Fe nanocomposites varies very slowly and exhibits relaxation type characteristic in the 0.5-18 GHz frequency range, and the second peak value of imaginary part μ_r'' obtains at 13GHz. The imaginary part of permittivity for the composites exhibits a peak at 9GHz. The dielectric properties of arise mainly from the interfacial polarization.

Fig.14 illustrates the frequency dependence of magnetic loss and dielectric loss in the range of 0.5-18GHz for $Nd_6Fe_{91}B_3$ composites. The magnetic loss shows two dispersion peaks and the dielectric loss show one peak value as well as relative permeability, permittivity in this frequency range. Consequently, microwave absorption properties of α-Fe/$Nd_2Fe_{14}B$ composites depend on cooperate effect of magnetic loss and dielectric loss.

Finally, the RL of $Nd_6Fe_{91}B_3$ composites are calculated from the microwave complex permeability and permittivity, and absorber thickness. Their frequency dependence is shown in Fig.15. This nanocomposite shows an excellent microwave absorption property (reflection loss: RL<-20dB) in 9-17GHz with thin matching thickness 1.6-2.5 mm. Therefore, α-Fe/$Nd_2Fe_{14}B$ nanocomposites are thought to be a potential candidate for thinner microwave absorbers in GHz range.

The permeability spectra of $Nd_2Fe_{14}B/\alpha$-Fe nanocomposites exhibits relaxation type characteristic in the 0.5-18 GHz frequency range. Microwave absorption properties of this composites depend on cooperate effect of magnetic loss and dielectric loss. A minimum RL of -37dB is observed at 16GHz with an absorber thickness of 1.6 mm. $Nd_2Fe_{14}B/\alpha$-Fe nanocomposites are promising microwave absorbers in GHz frequency range.

5. Effect of microstructure on microwave complex permeability of $Nd_2Fe_{14}B/\alpha$-Fe nanocomposites

The effect of ball milling process on the microstructure, morphology and microwave complex permeability of $Nd_2Fe_{14}B/\alpha$-Fe nanocomposites have been investigated. The mechanical ball milling can reduce the grain sizes and the particle sizes of $Nd_2Fe_{14}B/\alpha$-Fe nanocomposite material as shown in Fig.16 and Table 1, and the particle of powder becomes fine and thin, the grain size reduces during the process of milling. and enhance the microwave complex permeability and the complex permittivity. The effect of exchange interaction between the hard-magnetic $Nd_2Fe_{14}B$ and soft-magneticα-Fe enhance, its anisotropy fields H_A and saturation magnetization M_s increase as shown in Fig.17, and the microwave complex permeability increase and the resonance frequencies f_r shift to high frequency with proper ball milling time as shown in Fig.18. The optimal complex

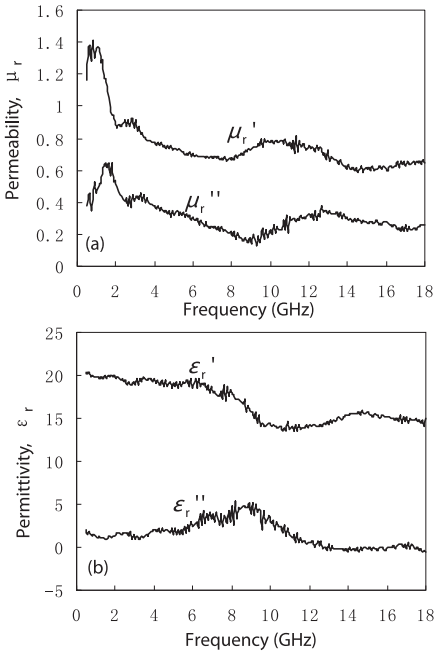

Fig. 13. Frequency dependence of relative complex permeability (a), permittivity (b) of $Nd_6Fe_{91}B_3$ compositions

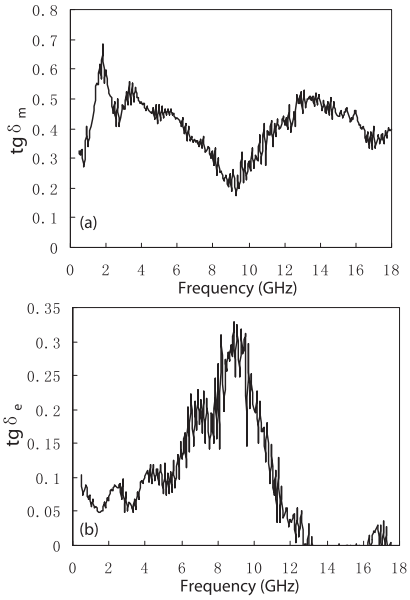

Fig. 14. Frequency dependence of dielectric and magnetic loss of $Nd_6Fe_{91}B_3$ compositions

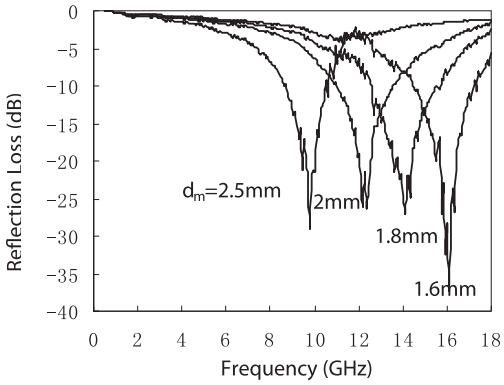

Fig. 15. Frequency dependence of reflection loss for $Nd_6Fe_{91}B_3$ compositions with different matching thickness

permeability are obtained after ball milling for 25h, and the maximum values of μ' is 2.6 at 3GHz, the maximum values of μ'' is 1.2 at 12GHz, and furthermore , the maximum values of μ'' is 0.85 at 30.5GHz. Thus the resonance frequencies f_r of $Nd_2Fe_{14}B/\alpha$-Fe nanocomposites can be controlled, and these novel materials can be used for microwaveabsorbers operating in both centimeter wave and millimeter wave. The ball milling process is an efficient way to optimize the microstructure and improve microwave electromagnetic properties of $Nd_2Fe_{14}B/\alpha$-Fe nanocomposites.

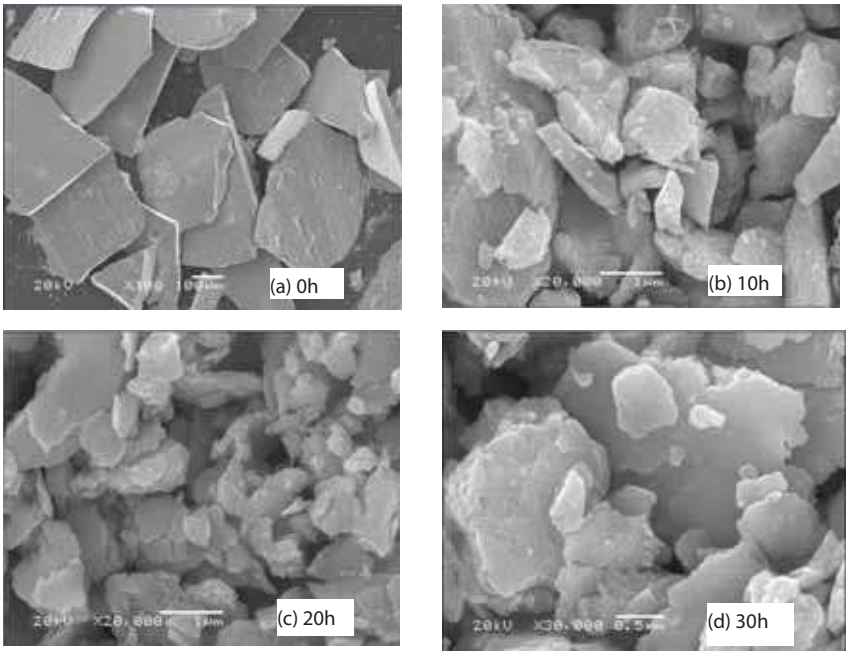

Fig. 16. SEM micrographs of $Nd_{10}Fe_{84}B_6$ composite with various milling time

	0h	10h	20h	30h
Powder size /μm	400	4.88	3.81	3.2
Grain size / nm	37	25	20	18

Table 1. Even size of powder and grain for sample after various milling time

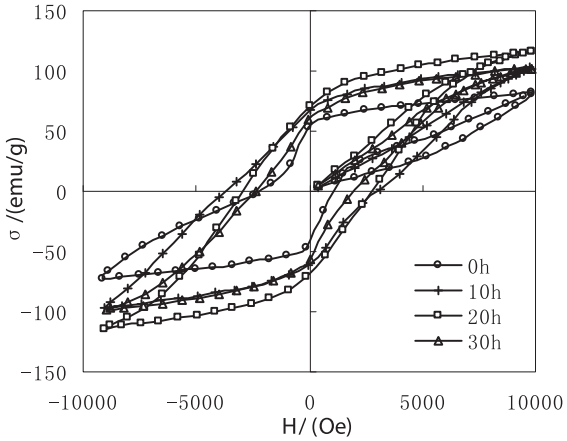

Fig. 17. Magnetic hysteresis loops for $Nd_{10}Fe_{84}B_6$ composite with various milling time

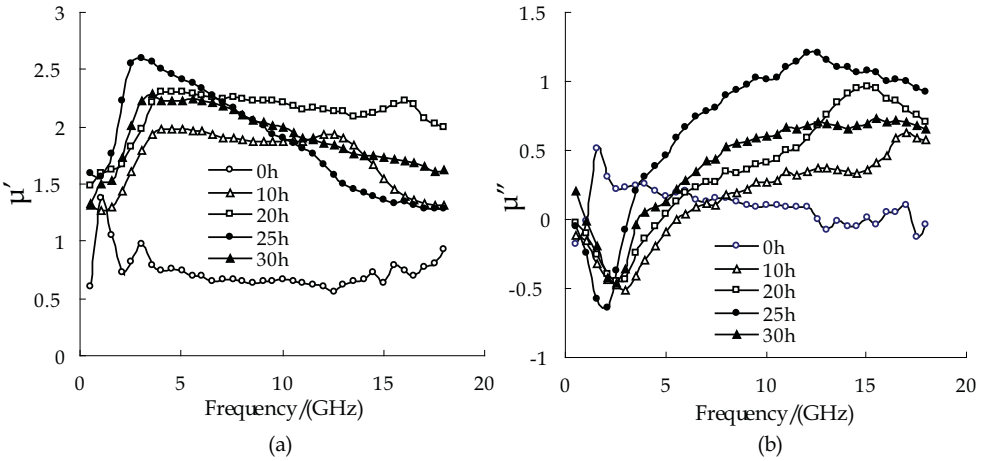

Fig. 18. The real part μ_r'(a) and imaginary part μ_r'' (b) of complex relative permeability against frequency for $Nd_{10}Fe_{84}B_6$ composite after various milling time in the 0.5-18GHz

III. Electromagnetic wave absorption properties of nano-crystalline SmN/α-Fe and SmO/α-Fe composite

In our early study on $Sm_2Fe_{17}N_x$ magnetic material, it showed that the Sm_2Fe_{17} compound disproportionates into a two-phase, α-Fe/SmH_2 microstructure after heating under a hydrogen atmosphere (hydrogen-disproportionation) at temperatures from 873 to 1173 K. A

nanometer scale lamellar structure composed of SmH_2 and α-Fe is obtained after a heat treatment at temperatures close to 873 K. However, at higher temperatures, the SmH_2 lamellae grow to form spheres several hundred micrometers in diameter, embedded within an α-Fe phase. If the disproportionated microstructure heated in nitrogen and then oxidation treatment in oxygen or air at lower temperature, a similar disproportionated microstructure of α-Fe/SmN and α-Fe/SmO finally can be obtained, due to the difference in free energy change for the formation of oxide between rare earth elements and iron. In addition, the SmO compounds exhibit a lager resistivity than RH_2 and SmN phase. Therefore, a similar disproportionated microstructure of α-Fe/SmO can be a EMI material with high microwave absorption properties. However, there are hardly reports relevant to the application of this effect for microwave absorbers. Therefore, in this chapter, the effect of the microstructure and preparation processes on EM wave absorption properties in GHz-range microwave absorption is investigated.

1. Preparation process and measurement

Fig.19 shows the preparation process.Sm_2Fe_{17} alloys were produced by industrial melting method with initial materials whose purities were 99.9% or above in argon atmosphere(see Fig.20). The ingot was annealed in argon atmosphere at 1323 K for 24h(see Fig.21). Then the homogenized ingot was crushed into powders of less than 100μm in size. The crushed Sm_2Fe_{17} powders were ball-milled into powders of about 10 μm for 20 minute. The Hydrogenation-Disproportion (HD)and nitrogen process were conducted as following: the crushed powders were placed in a furnace and heated to 875K at a rate of 5K/min in a high purity hydrogen atmosphere of 0.1MPa , held for an hour, Subsequently the furnace was vacuumized to $\times 10^{-4}$Pa and then cooled to 773K in a high purity nitrogen atmosphere of 0.3MPa, held for 5h.The nitrified powder was heated in oxygen or air (oxygen-disproportionation) at 573K for 2h.

X-ray diffraction (XRD) and transmission electron microscope (TEM) were used to determine the phases and microstructure of samples. The magnetic hysteresis loops were measured using a vibrating sample magnetometer (VSM)(see Fig.22). The alloy powders were mixed with paraffin at a weight ratio of 5:1 and compacted respectively into a toroidal shape (7.00 mm outer diameter, 3.01 mm inner diameter and approximately 3 mm thickness)The vector value of reflection/transmission coefficient (scattering parameters) of samples were measured in the range of 0.5-18 GHz, using an Agilent 8720ET vector network analyzer respectively. The relative permeability (μ_r) and permittivity (ε_r) values were determined from the scattering parameters and sample thickness. Assumed the metal material was underlay of absorber, and the reflection loss (RL) curves were calculated from the relative complex permeability and permittivity with a given frequency range and a given absorber thickness (d) with the following equations :

$$RL = 20\lg\left|(Z_{in}-1)/(Z_{in}+1)\right| \tag{1}$$

$$Z_{in} = \sqrt{\mu_r/\varepsilon_r}\tanh\left\{j(2\pi fd/c)\sqrt{\mu_r\varepsilon_r}\right\} \tag{2}$$

where Z_{in} is the normalized input impedance at absorber surface, f the frequency of microwave, and c the velocity of light.

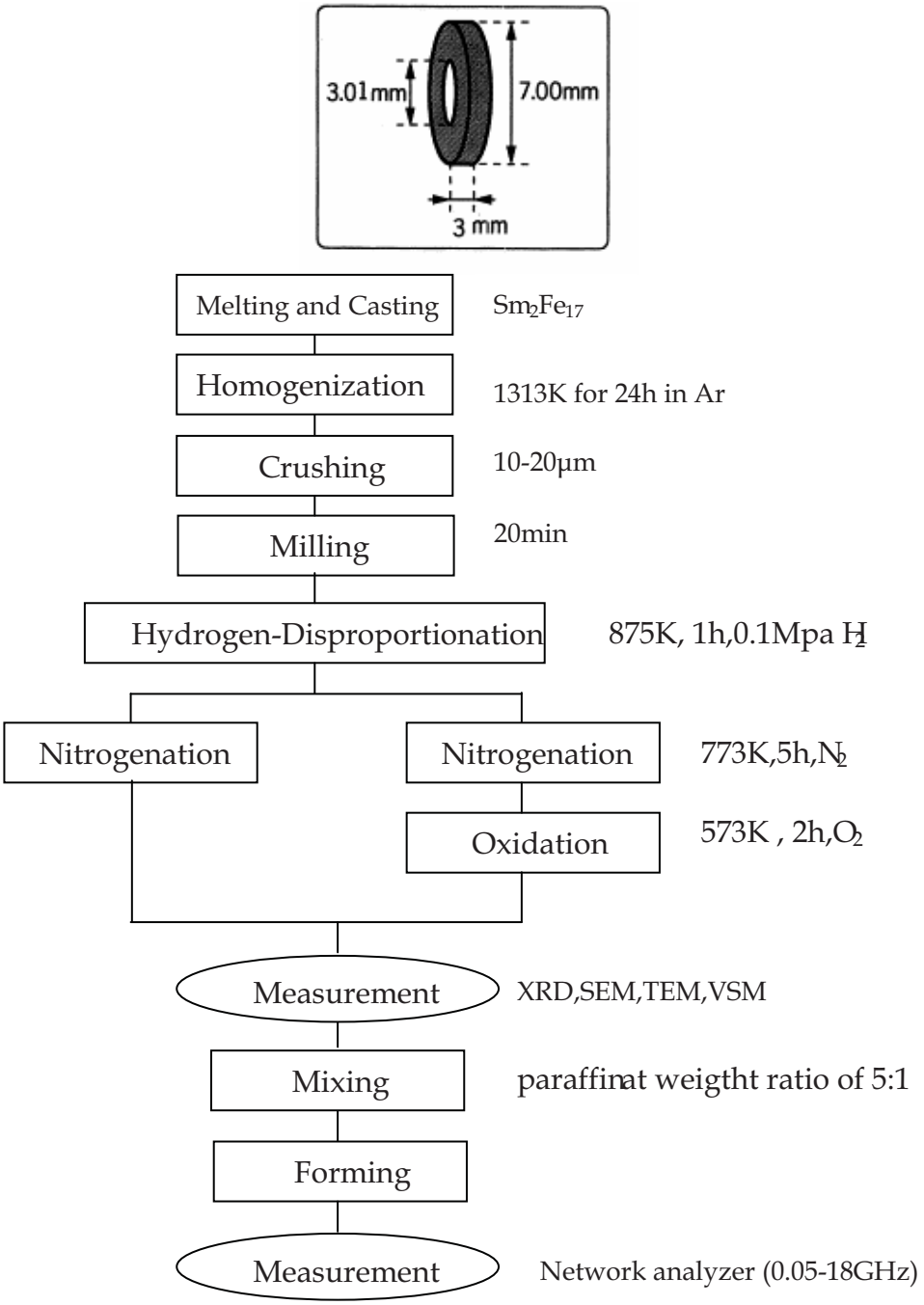

Fig. 19. Preparation procedure

Fig. 20. Medium frequence induction melting furnace

Fig. 21. Vacuum heat treatment furnace

Fig. 22. LakeShore7410 VSM

2. Microstructure of SmN / α-Fe and SmO / α-Fe phase coupling absorbing material

Fig. 23 shows X-ray diffraction patterns of the homogenized Sm_2Fe_{17} powders (a) , (b)after hydrogen-disproportionation at 873 K for 1 h , (c) followed by nitrified at 773 K for 5 h in0.3Mpa N_2, and (d) after oxygen-disproportionation at 573 K for 1 h. .It can be seen from Fig.23(a) that the main phase in as-homogenized ingot is Sm_2Fe_{17} with rhombohedra Th_2Zn_{17}-type structure ,co-existing with small fraction of Sm-rich and α-Fe phases. It is confirmed from Fig.23 b that after hydrogenation at 873K for 1h, the Sm_2Fe_{17} (113) peak almost can not be detected, and the alloy is almost composed of SmHx and α-Fe phase. It suggests that disproportation completed according to the reaction:

$$Sm_2Fe_{17}+H_2 \rightarrow \quad SmH_x + \alpha\text{-Fe} \qquad (3)$$

Fig.24 shows TEM image and diffraction patterns of SmH_x/α-Fe. It can be seen that a nanometer scale lamellar structure composed of SmH_2 and α-Fe is obtained after a heat treatment at temperatures close to 873 K according to diffraction pattern. Also, as local high temperature in the sample, the SmH_2 lamellae grow to form spheres several hundred micrometers in diameter, embedded within an α-Fe phase. The top left corner of the picture in Fig.24 is to enlarge the box office chart, from which can be drawn that the growth of the alloy grains and the dimensions of the grains are about 10nm. These correspond to the result of XRD analysis. After nitrified at 773 K for 5 h , the SmH_x phase is completely transformed into SmN phase, while the α-Fe phase content is essentially the same(see Fig.23c).Thus the electromagnetic wave absorption materials with SmN/α-Fe phase coupling structure were obtained. When the powder with SmN/α-Fe two-phase structure heated in the air after 1 h, it can be seen from Fig.23(d), that the alloy is composite of SmO and α-Fe phase, oxide of iron is not detected ,namely SmN phase has transformed into SmO. The difference of diffraction peak between SmN (PDF 30-1104) and SmO (PDF 65-2915) is not obvious. The characteristic diffraction peaks were enlarged in the diagram at the upper left corner of Fig.23, it illustrate that the position of two diffraction peak are different at enlarged picture. Combined with the color change of oxidized powder before and after, all of these confirmed again that SmN phase has been changed into SmO phase.

Fig.25 is SEM picture of nitrified and oxidized powder of SmFe alloy. It Shows that each particle size is between 1 ~ 5 μm. Small particles can reduce the eddy current, and then helps to reduce magnetic permeability induced by eddy current. Compared with SmN phase, the resistivity of SmO phase is lager, which can increase skin depth of eddy current, and further reduce the eddy current. Otherwise, this structure can generate an exchange coupling effect, which is conducive to increase the natural vibration frequency of materials.

3. Electromagnetic wave absorption properties of SmN / α-Fe and SmO / α-Fe composites

Fig.26 shows the frequency dependence of the complex relative permeability and permittivity of SmN / α-Fe and SmO / α-Fe composites. As shown in Fig.26(a), that the real part of complex permittivity ε_r (= ε_r - $j\varepsilon_r$) decre ε_r ase with increasing frequency for SmN / α-Fe and SmO / α-Fe composites in 0.5-18 GHz, and that of the nitrified and oxidized sample remains almost constant in the frequency range of about 9HGz. But the relative

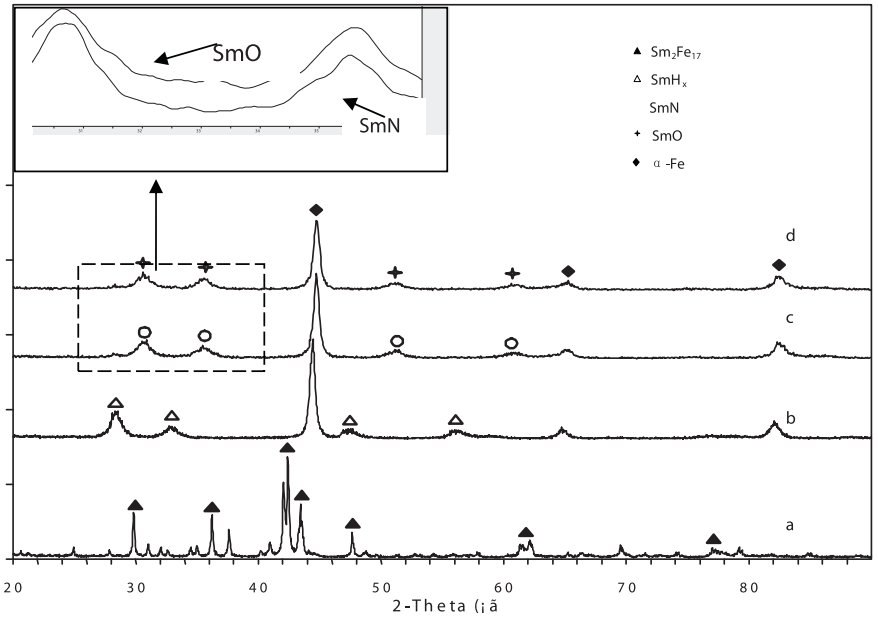

Fig. 23. The XRD patterns of Sm_2Fe_{17}: (a) homogenized powders, (b) after hydrogenation-disproportionation at 873 K for 1 h in H_2, (c) after nitriding the sample (b) at 773 K for 5 h, and (d) after oxidizing the sample (c) in O2 at 573 K for 1 h

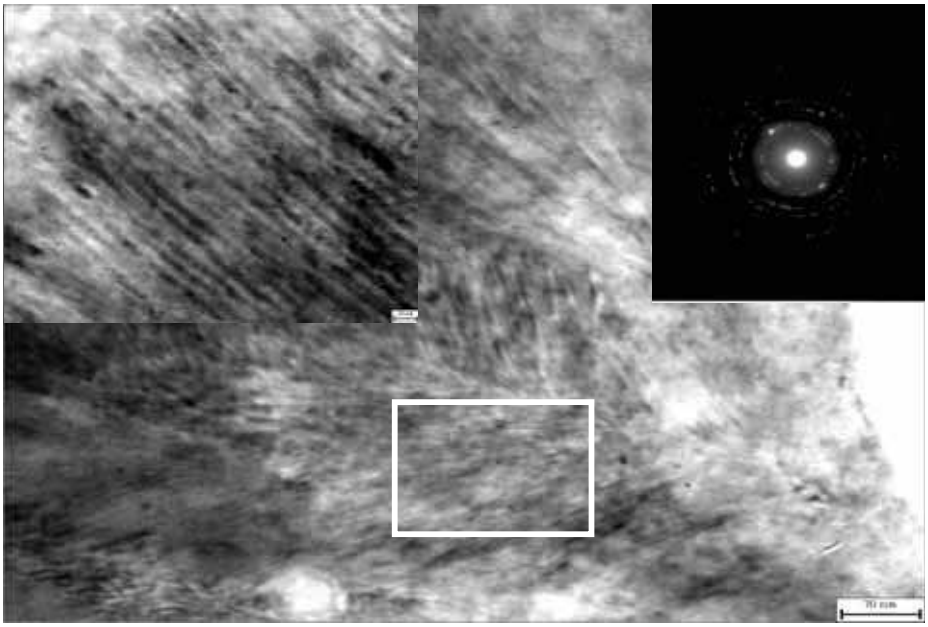

Fig. 24. TEM image , diffraction patterns of SmHx/α-Fe and enlarge picture

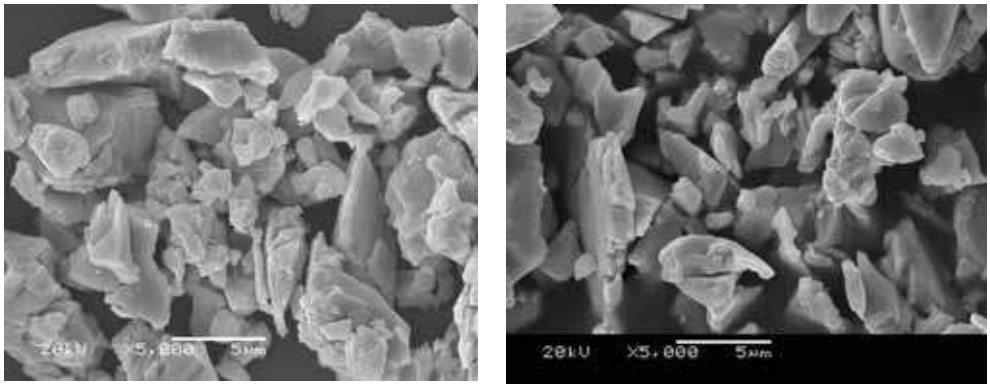

(a) (b)

Fig. 25. SEM image of SmN/α-Fe and SmO/α-Fe composites (a) SmN/α-Fe composite;(b) SmO/α-Fe composite

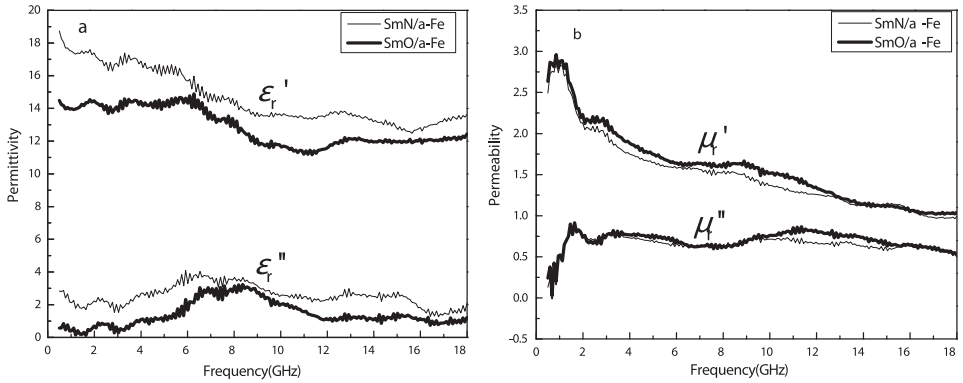

Fig. 26. (a)The relative permittivity plotted against frequency for SmN/α-Fe and SmN/α-Fe composites in the 0.5-18GHz. (b) The relative permeability plotted against frequency for SmN/α-Fe and SmO/α-Fe composites in the 0.5-18GHz

permittivity ε_r'' exhibits a peak at the frequency nearly 8HGz. As can be seen from Fig. 26 (b) ,that complex permeability of SmN/α-Fe and SmO/α-Fe composites are similar, the real part of complex permeability μ_r' show maximum of value 3.2 at a frequency of 1GHz.While the relative permeability μ_r'' have two peaks, and remain a high value in a wide frequency band. It found that it shows the phenomenon of multiple resonances for Fe-Co-Ni bonded composite elastic material with the Fe-Co-Ni powder particles decreased from micron to sub-micron. As to SmN/α-Fe and SmO /α-Fe composites, because that its powder particle is uniform and size distribution is between the 1-5μm (see Fig.25), the relative permeability exhibits two peaks in the 0.5-18GHz, which is the characteristics of the multiple resonance.
In addition, it can be found from Fig.8 that the real part and relative permittivity of SmO/α-Fe composite are lower than that of SmN/α-Fe composite. This is ascribed to the lower

resistivity of SmN than SmO phase's, due to the permittivity of SmN/α-Fe composite being lager, and more fluctuations with the frequency. As we all know, the relative permeability can express by the formula (4):

$$\mu_r^{''} = \frac{M_s}{3\mu_0 H_A \alpha} \quad (4)$$

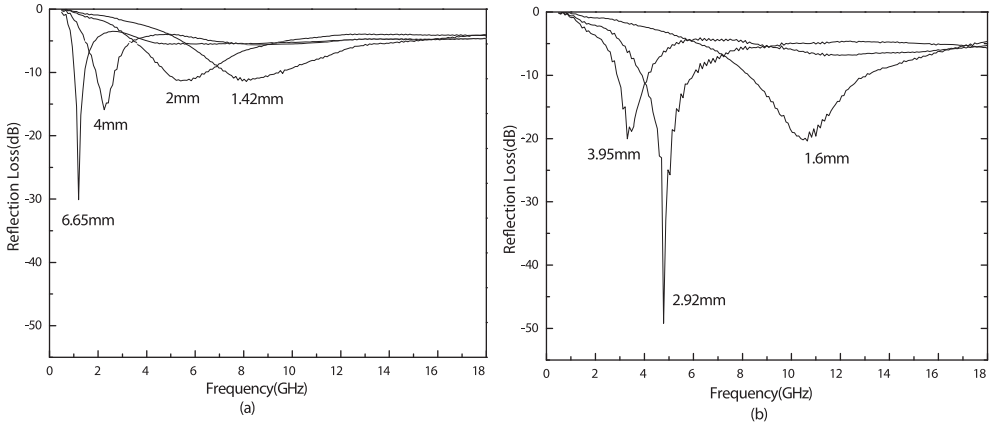

Fig. 27. Frequency dependences of RL of SmN/α-Fe and SmO/α-Fe composites at different thicknesses.(a) SmN/α-Fe composite;(b) SmO/α-Fe composite

where M_s is saturation magnetization, μ_0 is vacuum permeability, H_A is anisotropy magnetic field,αis constant. Also, their complex permeability are similar according to Fig.26, which are main contribute to α-Fe in the two materials. It can be calculated by XRD patterns (Fig.23)that the content of α-Fe content in the two materials are almost identical, which is confirm by VSM measurement with saturation magnetization value of 120 emu/g for SmN/α-Fe and SmO/α-Fe composites. As can be seen from Fig.26(b) , the permeability of SmO/α-Fe composite is slightly higher in fact. The reason is that the resistivity increases during the SmN phase transform to SmO phase, due to reduce the eddy current and decreased slowly the permeability with increase of frequency. It can be drawn from the formula (1) that in order to achieve full non-reflective, that is, R = 0, the value of complex permittivity and complex permeability for the absorbing materials must be equal, that is to say , the normalized input impedance at absorber surface Z_{in}= 1. Hence, high-performance absorber material is characterized by as possible to keeping both permeability and permittivity approximately equal at a wide frequency range. It can be deduced that SmO/α-Fe composite have better absorbing performance from the permeability and permittivity in Fig.26.

Figure 27 shows frequency dependences of RL of SmO/α-Fe composite at different thickness. It can be seen that the two materials in the 0.5-18 GHz have good absorbing properties, with the absorbing coating thickness increases, the minimum reflection loss of absorber moves to the low frequency. Because the match between the permeability and the dielectric constant for SmO/α-Fe is better than that for SmN/α-Fe, the former has better EM wave absorption property and its RL (reflection loss) is less than –20 dB with absorber

match thickness of 1.60~3.95 mm in the frequency range of 3.30~10.65 GHz. The minimum RL is –50 dB, absorber match thickness is 2.92 mm at 4.8 GHz.

4. Acknowledgements

This work is supported by National Natureal Science Foundation of China (No.10804079) and Doctoral Fund for New Teachers No. 15205025 from the Ministry of Education of China.

5. References

[1] J.L. Snoek, Physica 14, 207(1948).
[2] D. Rousselle, A. Berthault, O. Acher, et al. [J] J. Appl. Phys.,74,475(1993).
[3] E.P. Wohlfarth, K.H.J. Buschow, in: Ferromagnetic Materials, Vol.4, Elsevier Science Publishers B.V., Amsterdam, 1988.
[4] H. Ono, T. Tayu, N. Waki, et al. [J] J. Appl. Phys.,93,4060(2003).
[5] L.X. Lian, L.J. Deng, M. Han, et al. [J] J. Alloys Compd., 441, 301 (2007).
[6] Li-Xian Lian, L. J. Deng, and M. Han. [J] J. Appl. Phys., 101, 09M520 (2007).
[7] Chen Xianfu, Ye Jinwen, Liu Ying, et al. [J] Rare Metal Materials and Engineering,38, 726(2009).
[8] Y. Naito, K. Suetake, IEEE Trans. Microwave Theory Tech. MTT-19, 65(1971).
[9] C.Sudakar, G.N.Subbanna, and T.R.N.Kutty. [J] J. Appl. Phys., 94, 6030(2003).
[10] E. F. Kneller, R. Hawig, IEEE Trans. Magn. 27, 3588 (1991).
[11] R. Skomski, J. M.D. Coey, Phys. Rev. B., 48, 15812(1993).
[12] Y. J. Kim and S. S. Kim, IEEE Trans. Mag., 38, 3108(2002).
[13] T. Maeda, S. Sugimoto, T. Kagotani, Nobuki Tezuka, Koichiro, J. Magn. Magn. Mater.281, 195 (2004).
[14] R. Gerber, C.D. Wright, G. Asti (Eds.), Applied Magnetism, Kluwer Academic Publisher, Doldrecht, pp.457(1992).
[15] E.P. Wohlfarth, K.H.J. Buschow, in: Ferromagnetic Materials, Vol.4, Elsevier Science Publishers B.V., Amsterdam, (1988).
[16] H. Kato, M. Ishizone, T. Miyazaki, K. Koyame, H. Nojiri, M. Motokawa, IEEE Trans. Magn. 37, 2567(2001).
[17] J. Jakubowicz, M.Giersig, J Alloys Compounds, 349, 311(2003).
[18] L.X. Lian, Y. Liu, S.J. Gao, M.J. Tu, J. Rare Earths, 23(2), 203(2005).
[19] I. Panagiotopoulos, L. Withanawasam, A.S. Murthy, G.C. Hadjipanayis, J.Appl. Phys. 79, 4827(1996).
[20] J. Jakubowicz, M. Jurczyk, J. Magn. Magn. Mater., 208, 163(2000).
[21] J. Bauer, M. Seegrer, A .Zern, H. Kronmüller, J. Appl. Phys., 80 , 1667(1996).
[22] T. Schrefl, J. Fidler, H. Kronmüller, Phys.Rev.B., 49, 6100 (1994).
[23] T. Leineweber, H. Kronmüller, J. Magn. Magn. Mater., 176, 145(1997).
[24] C.Sudakar, G.N.Subbanna, and T.R.N.Kutty. [J] J. Appl. Phys., 94, 6030(2003).
[25] Koji Miura, Masahiro Masuda, etc. [J].Journal of Alloys and Compounds 408–412, 1391(2006).
[26] Zhou Shouzeng,Dong Qingfei. Super Permanent Magnets [M]. BeiJing: Metallurgy Industry Publishing House, 406,(1999).
[27] YE Jinwen, Liu Ying, Gao Shengji, Tu Ming-jing. [J].Journal of theChinese Rare Earth Socity. 23(3):303(2005).

[28] YE Jinwen, Liu Ying, Gao Shengji, Tu Ming-jing. [J].Rare Metal Materials and Engineering, 34(12): 2002(2005).
[29] Coey J M D, Sun H, Otani Y. Proceeding of 11th Int. Workshop on RE Magnets and their applications, 36~40(1990).
[30] Li Fang, Liu Yingetc. [J]. Metaltlc Functional Materlals. 11(3)(2004).
[31] S.Sugimoto,T.Kagotani etc. [J] Journal of Alloys and Compounds 330–332, 301 (2002).
[32] Jiu Rong Liu, Masahiro Itoh, Jianzhuang Jiang, Ken-ichi Machida. [J].Journal of Magnetism and Magnetic Materials 271, L147 (2004).

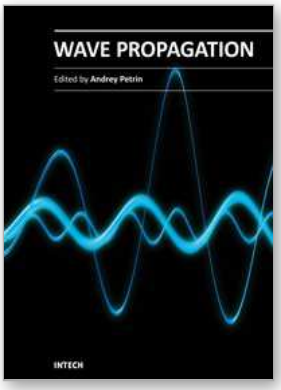

Wave Propagation
Edited by Dr. Andrey Petrin

ISBN 978-953-307-275-3
Hard cover, 570 pages
Publisher InTech
Published online 16, March, 2011
Published in print edition March, 2011

The book collects original and innovative research studies of the experienced and actively working scientists in the field of wave propagation which produced new methods in this area of research and obtained new and important results. Every chapter of this book is the result of the authors achieved in the particular field of research. The themes of the studies vary from investigation on modern applications such as metamaterials, photonic crystals and nanofocusing of light to the traditional engineering applications of electrodynamics such as antennas, waveguides and radar investigations.

InTech Europe
University Campus STeP Ri
Slavka Krautzeka 83/A
51000 Rijeka, Croatia
Phone: +385 (51) 770 447
Fax: +385 (51) 686 166
www.intechopen.com

InTech China
Unit 405, Office Block, Hotel Equatorial Shanghai
No.65, Yan An Road (West), Shanghai, 200040, China
中国上海市延安西路65号上海国际贵都大饭店办公楼405单元
Phone: +86-21-62489820
Fax: +86-21-62489821